Atomically homogeneous dispersed ZnO/N-doped nanoporous carbon composites with enhanced CO_2 uptake capacities and high efficient organic pollutants removal from water

Binling Chen [a], Guiping Ma [a,b], Dali Kong [a], Yanqiu Zhu [a], Yongde Xia [a,*]

[a] *College of Engineering, Mathematics and Physical Sciences, University of Exeter, Exeter EX4 4QF, United Kingdom*

[b] *State Key Laboratory of Chemical Resource Engineering, Beijing Laboratory of Biomedical Materials, Beijing University of Chemical Technology, Beijing 100029, PR China*

[*] Corresponding author.

Email address: y.xia@exeter.ac.uk (Y. D. Xia).

ABSTRACT

Advanced functional composite of ZnO nanoparticles embedded in N-doped nanoporous carbons has been synthesized by a simple one-step carbonization of zeolitic imidazolate framework-8 under a water stream atmosphere. A variety of characterization techniques show that the introduction of water steam during the carbonization process holds the key to obtain the fine and homogeneously dispersed ZnO nanoparticles within the functionalised nanoporous carbon matrix. Possessing a higher specific surface area, a larger pore volume and abundant oxygen-containing hydrophilic functional groups, the resulting composite exhibits a stronger interaction with CO_2 and is more efficient to promote the photocatalytic degradation-adsorption of methylene blue under visible light than the composite obtained without steam treatment. As a result, the steam derived composite exhibits increased CO_2 uptake capacity and excellent methylene blue molecules removal from water. Using different metal-organic frameworks as precursors, this new, simple and green method can be further expanded to generate various new homogeneous dispersed functional metal oxide/porous carbon composites with high efficient in relevant applications.

1. Introduction

Porous carbon materials with high specific surface area, large pore volume, narrow pore-size distribution, good chemical and thermal resistance, and affinity to organic contaminations are very promising for many applications,[1-4] particularly being widely used in air and water purification, gas storage, catalysts, and eletrochemical devices.[5-8] After enormous efforts have been devoted to this field in recent years, the pore structures of carbons at micropore or mesopore levels can be readily controllable via various synthesis approaches.[9-11]

Recently, porous carbon–metal oxide composite materials have attracted huge interest due to their promising potential in environmental applications, such as gas sorption and contamination removal from water. Reducing CO_2 emission has become a key environmental challenge since CO_2, one of the main greenhouse gases and mainly generated from the combustion of fossil fuels, has been widely recognised as a main contributor to global warming. For instance, mesoporous carbon-MgO composites have showed high efficiency for CO_2 capture.[12, 13] In addition, removal of organic pollutants from industrial and household wastewater is also an important environment issue and carbon-semiconductor composites have been explored for organic pollutants removal from wastewater.[14-17] For example, porous carbon-TiO_2 composite acts not only as a photocatalyst under visible light and showed good photodegradation activity for organic pollutants, but also as an adsorbent to extract the pollutants through the pores of the matrix.[14-16] Similarly, porous carbon-doped ZnO composite also exhibited a good photocatalytic performance in terms of the degradation of organic pollutants under visible light.[17, 18]

However, the components in these porous carbon-metal oxide composites usually cannot achieve homogeneous dispersion since they were frequently prepared by mechanical or physical mixing the metal oxides with the porous carbon materials. More recently, metal

organic frameworks (MOFs) (including Zeolitic Imidazolate Frameworks (ZIFs)), a new class of inorganic-organic crystalline nanoporous materials that assembled from metal ions coordinated to rigid organic ligands,[19, 20] have emerged as promising precursors or sacrificial templates for the preparation of porous carbon based materials,[21, 22] due to their tuneable structures, vast functionalities and fascinating properties. The preparation procedure is simple, and porous carbon-based materials can be produced by the direct carbonization of MOFs in an inert atmosphere, without any additional carbon precursors. Due to the inorganic-organic crystal structure of the parental MOFs, the generated metal or metal oxide can be remained homogeneously within the nanoporous carbon matrix.[21] To date, only a few reports have adopted such a thermal treatment of MOFs route for the fabrication of composites. Das *et al* reported a generalized strategy for the synthesis of crystalline metal oxide nanoparticles embedded in a carbon matrix by a controlled thermolysis of MOFs.[23] Yamauchi *et al* demonstrated that the creation of nanoporous carbon–Co_2O_3 hybrid materials via a two-step thermal conversion of ZIF-9,[24] while Guangju *et al* obtained N-doped carbon-Co_3O_4 composites using a one-step thermal conversion from a specific MOF, Co–I–MOF.[25] Most recently, we utilized a typical sodalite topology ZIF-8, which is built from corner-shared tetrahedral ZnN_4 units and the coordination bonds between the Zn^{2+} ions and 2-methylimidazole anions that are amongst the most stable N-donor ligands,[26] to synthesize ZnO/porous carbon composites by the direct carbonization in argon atmosphere, but no XRD peaks related to either ZnO or Zn can be observed in these composites.[27] Therefore, designing new synthesis strategies to create efficient porous carbon-metal oxide composites is highly desirable.

Water is a natural green solvent and water steam has been widely considered as a weak oxidizing agent that can benefit to the slow oxidation rate. Therefore, such a mild and fine controllable oxidation process will not compromise the properties of target materials. This

becomes particularly true when water steam is used as an oxidation agent during the generation of porous carbon-metal oxide composites since water steam can react with and oxidise carbons at high temperatures. Inspired by these facts, in this work, a mild and green one-step oxidation approach using water steam at high temperatures has been developed and demonstrated its promising effectiveness in the utilisation of ZIF-8 as a single precursor to generate atomically homogeneous dispersed ZnO/nanoporous N-doped carbon composites, which exhibited excellent CO_2 uptake capacities, efficient adsorption and photodegradation performance in the removal of methylene blue (MB) from water under visible light irradiation.

2. Experimental

2.1 Materials synthesis

ZIF-8 was synthesized from zinc nitrate hexahydrate and 2-methylimidazole in methanol solution, following an established procedure.[28] The porous composites were prepared by a one-step direct carbonization process in the presence of water steam. In a typical synthesis, an alumina boat with 0.25 g of dried ZIF-8 was placed in the centre of a flow-through quartz tube sitting in a tube furnace. The furnace was heated at 10 ^{o}C /min to the target temperature (typically 800 °C) under pure argon; when the furnace temperature reached 800 ^{o}C, a 20 ml/min of argon flow saturated with water vapour was introduced in and maintained at the target temperature for 3 h. The gas flow was then switched to argon only while the furnace cooled to room temperature. The final product was collected from the quartz tube and labelled as ZnO/C-S-*S*. Another sample was also obtained via the similar one-step direct carbonization process where a 20 ml/min of argon flow saturated with water vapour is constantly presented during the heating up step, the maintaining at the target temperature for 3 h and the cooling down to room temperature. This sample was designed as ZnO/C-S-*L*. For comparison, the one-

step process was also applied to the annealing of ZIF-8 at 800 ^{o}C for 3 h under argon atmosphere with a flow rate of 20 ml/min,[27] and the collected samples was named as ZnO/C-A. A pure ZnO was also obtained via annealing of ZIF-8 in air at 800 ^{o}C for 3 h.

2.2 Material characterizations

X-ray diffraction (XRD) patterns were recorded with a Cu Kα radiation (40 kV-40 mA) at a step time of 1 s and a step size of 0.02^{o}. Fourier-transform infrared (FTIR) spectra were obtained using an Alpha Bruker system. The samples were measured in the wavenumber range of 2000–500 cm^{-1}. The Raman spectra of the samples were recorded in the backscattering arrangement, using a 532 nm laser excitation under laser power of 6 mW. Thermogravimetric analysis (TGA) was performed on a TA SDT Q600 instrument from the room temperature to 800 ^{o}C with a heating rate of 10 ^{o}C min^{-1} under a continuous air flow of 100 mL min^{-1}. A Hiden QGA gas analysis mass spectrometer (MS) was coupled with the Q600 instrument to monitor and detect the gaseous compositions in the exhaust emission. Transmission electron microscopy (TEM) images and elemental mapping analysis were obtained on a JOEL-2100 at an acceleration voltage of 200 kV. The powder samples were first dispersed in absolute ethanol under moderate sonication, then pipetted onto a holey carbon Cu grid to obtain TEM specimens. N_2 gas sorptions were carried out on a Quantachrome Autosorb-iQ gas sorptometer via the conventional volumetric technique. Before gas analysis, the sample was evacuated for 3 h at 200 °C under vacuum. The textural properties were determined via N_2 sorption at -196 °C. The surface area was calculated using the Brunauer-Emmett-Teller (BET) method based on adsorption data in the partial pressure (P/Po) range of 0.02-0.22 and the total pore volume was determined from the amount of nitrogen adsorbed at P/Po of *ca*. 0.99. Micropore surface area and micropore volume were obtained via *t*-plot analysis. The pore size distribution (PSD) was given by the non-local density functional theory (NLDFT) method for slit/cylinder pores using

the software provided by Quantachrome. The fitting error was typically in the range of 0.5 − 1.0%. A Jenway 6715 UV/Vis spectrophotometer machine was used to obtain the UV-Vis diffuse reflectance spectra. X-ray photoelectron spectroscopy (XPS) was performed using a Kratos AXIS ULTRA spectrometer with a mono-chromated Al KR X-ray source (1486.6 eV) operated at 10 mA emission current and 15 kV anode potential. The analysis chamber pressure was better than 1.3×10^{-12} bar. The take-off angle for the photoelectron analyzer was 90^{o}, and the acceptance angle was 30^{o} (in magnetic lens modes). The luminescence properties were studied by photoluminescence (PL) spectroscopy using an Edinburgh Instruments Spectrofluorometer FS5. The excitation wavelength was 350 nm.

2.3 CO_2 uptake measurement

CO_2 gas adsorption capacities were investigated on a Quantachrome Autosorb-iQ gas sorptometer via the conventional static volumetric technique. Prior to the gas adsorption analysis, the samples were evacuated at 200 °C for 5 h under vacuum, then the CO_2 uptake measurements were carried out at 0 and 25 °C.

2.4 Adsorption and photodegradation evaluation

Adsorption capacity on the removal of methylene blue (MB) in water solution for the as-prepared ZnO/C composites was evaluated in a dark box. In details, 20 mg of as-prepared sample was added to 100 mL of 20 ppm MB solution, and the suspension was immediately kept in the dark box under stirring. At predetermined time intervals, a small amount of suspension was taken out and the concentration of MB in the solution was monitored by the UV–vis spectrophotometry. Similarly, the synergistic effect of adsorption and photocatalytic activities of the ZnO/C samples under the irradiation of visible light was also evaluated. 20 mg of sample dispersed in 100 mL of 20 ppm MB solution was immediately subjected to visible

light and the concentration of MB in the solution was monitored at designed time intervals. The visible light (cutoff filter applied, $\lambda > 420$ nm) was provided by 10 lamps of 20W (PerfectLight, wavelength range: 320 nm $\leq \lambda \leq$ 780 nm, light intensity: 160 mW/cm^2).

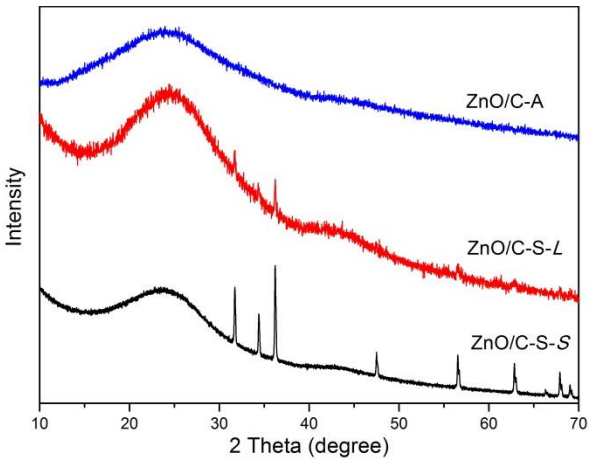

Fig. 1 - Powder XRD patterns of the composites of ZnO/C-S-*S*, ZnO/C-S-*L* and ZnO/C-A.

3. Results and discussion

3.1 Characterizations of the composites

The sodalite structure of the precursor ZIF-8 was firstly confirmed by XRD in Fig. S1a and the crystal structures of the as-synthesized ZnO/C composites were characterized by XRD and presented in Fig. 1. The sample ZnO/C-S-*S* which derived from water vapour carbonization of ZIF-8 for shorter period (3 h) shows XRD peaks at 2θ of 31.7°, 34.3°, 36.2°, 47.4°, 56.5°, 62.7°, 66.3°, 67.9° and 69.0°, which can be assigned to (100), (002), (101), (102), (110), (103), (200), (112) and (201) of ZnO with polycrystalline wurtzite structure (Zincite, JCPDS 5-0664). The ZnO/C composite derived from water vapour carbonization of ZIF-8 for longer duration

(sample ZnO/C-S-*L*), exhibits the main XRD peaks from wurtzite ZnO with reduced peak intensities. However, the sample derived from the carbonization in argon (sample ZnO/C-A) displays no peaks from ZnO, which is consistent with our previous observation.[27] Clearly the carbonization atmosphere has significant effect on the resulting composites. In addition, all the ZnO/C composites exhibit a broad XRD peak centred at the 2θ of 25° due to the (002) diffraction of carbon, indicating that the utilization of water vapour atmosphere does not damage the formation of porous carbon from ZIF-8 precursors.

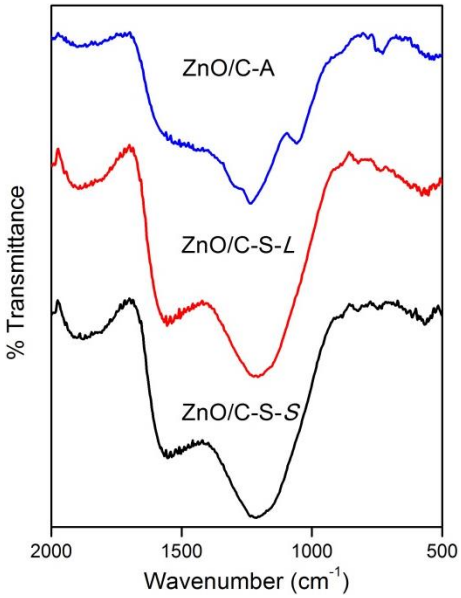

Fig. 2 - FTIR spectra of the composites of ZnO/C-S-*S*, ZnO/C-S-*L* and ZnO/C-A.

FTIR is an excellent technique for monitoring the presence of different functionalities on the surface of the composites. As shown in Fig. 2, sample ZnO/C-A derived from the carbonization in argon atmosphere displays broad peaks at 1210 cm^{-1} that can be assigned to C–C, C–N stretch while the 1580 cm^{-1} peak may come from aromatic C=C, C=N stretch of N-

doped carbon. A shoulder peak at around 1057 cm^{-1} can be due to the Zn-N stretching. For the composites derived from steam carbonization, however, a strong asymmetric peak centred at 1205 cm^{-1} is the contribution from the C-O stretch as well as the C-C and C-N stretch. The peak at 1580 cm^{-1} is stronger than in sample ZnO/C-A owing to the bending vibration of Zn-O-H bonding coupled with the contribution of C=C and C=N stretch from carbon, and Zn-O stretching model is clearly observed at 555 cm^{-1}. Moreover, an asymmetric peak between 1650–1850 cm^{-1} was observed for the steam carbonized samples, likely corresponding to the stretching vibration of C=O from the –COOH. In addition, a peak located at 3600-3700 cm^{-1} is attributed to the stretching of O-H groups from the Zn-OH or adsorbed water.[29] These observations clearly demonstrate that steam carbonization of ZIF-8 results in the formation of ZnO crystals and N-doped carbons with –COOH and –OH functional groups.

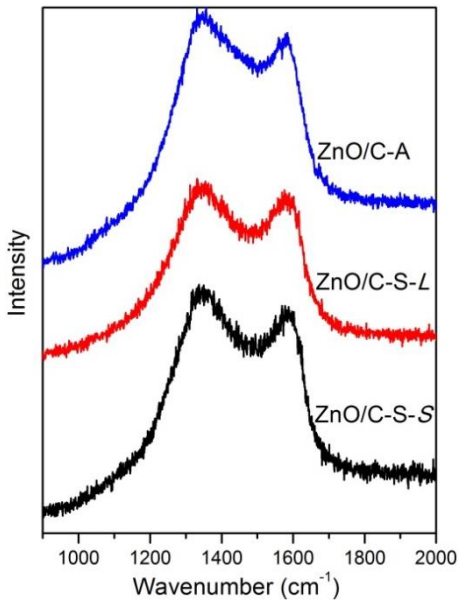

Fig. 3 - Raman spectra of the ZnO/C-S-*S*, ZnO/C-S-*L* and ZnO/C-A samples.

In the Raman spectra of the as-synthesized ZnO/C composites, the G band and D band are clearly seen as shown in Fig. 3, due to the bond stretching of all pairs of sp^2 atoms in both

rings and chains and the breathing modes of sp^2 atoms in rings, respectively.[30, 31] The G band at around 1590 cm^{-1} supports the presence of some nanocrystalline carbon and a high content of sp^2-hybridized carbon atoms caused by the carbonization of the samples. The D band at around 1350 cm^{-1} is an indication of less disordered carbon. Therefore, the relative higher I_D/I_G values of 0.89 and 0.96 for sample ZnO/C-S-*S* and ZnO/C-S-*L* respectively than that of 0.82 for sample ZnO/C-A, not only indicates the formation of abundant defects and amorphous carbons during the annealing process under both water steam and argon atmosphere,[32] but also suggests that ZnO/C composites derived from water steam carbonization possess more defects than that derived from argon atmosphere due to the weak oxidation capacity of high temperature water steam.

Table 1 - Textural properties, composition contents and CO_2 uptake capacities of ZnO/C composites derived from the direct carbonization of ZIF-8 under different conditions.

Sample	Surface area[a] / $m^2\ g^{-1}$	Pore volume[b] / $cm^3\ g^{-1}$	N content[c] / wt%	CO_2 uptake[d] / mmol g^{-1}
ZnO/C-S-*S*	995 (895)	0.58 (0.41)	8.1 (7.8)	3.05 (5.32)
ZnO/C-S-*L*	1134 (986)	1.06 (0.45)	11.6 (10.4)	3.23 (6.08)
ZnO/C-A	771 (706)	0.41 (0.33)	16.5 (14.4)	2.85 (4.42)

[a] The data in parenthesis are microporous surface area; [b] The values in parenthesis are micropore volume.; [c] Data in parenthesis are obtained from XPS analysis; [d] Data obtained at 25 ^oC and 1 bar, while the values in parenthesis are measured at 0 ^oC and 1 bar.

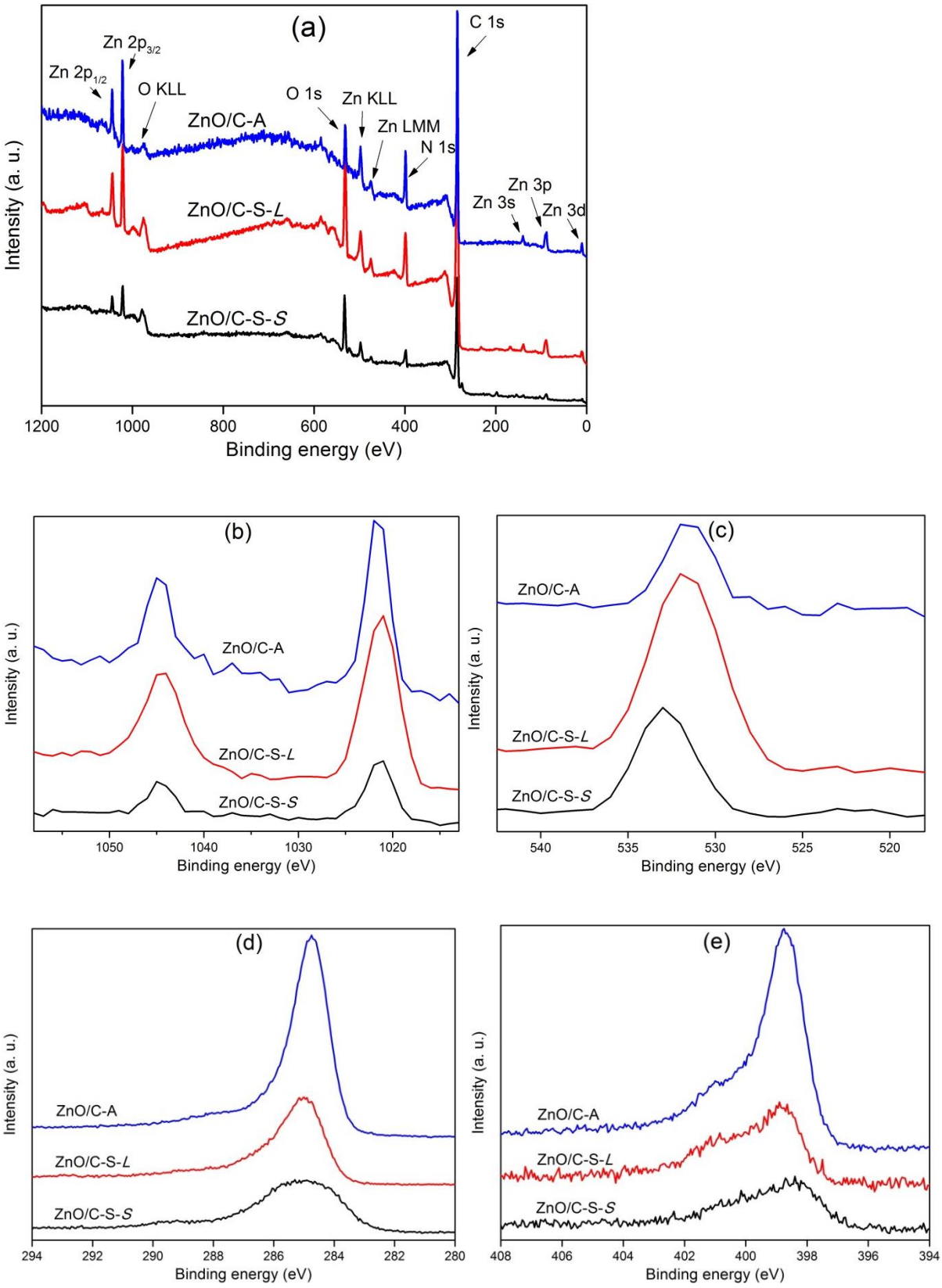

Fig. 4 - XPS results of (a) elemental survey, (b) Zn 2p, (c), O 1s, (d) C 1s and (e) N 1s for samples derived from carbonization of ZIF-8 at 800 ^{o}C under different conditions.

As presented in Fig. 4a, the elemental survey by XPS of the as-synthesized composites confirms the presence of C, N, Zn and O in all the samples. The Zn 2p spectrum contains a doublet at binding energy of 1021.8 and 1044.5 eV (Fig. 4b), assigned to Zn 2p3/2 and 2p1/2 lines, respectively. The binding energy distance between these two lines is 22.7 eV, indicating that the Zn ions in the composites are of a +2 state. As shown in Fig. 4c, the O 1s spectrum exhibited the bonding energy peaked at 531.8 eV, which can be assigned to O^{2-} ions in the Zn–O bonding of the wurtzite ZnO structure.[33] Moreover, the main peak for O 1s spectra can be deconvoluted into three peaks centred at 530.7, 532.1 and 533.2 eV, which can ascribe to the contribution from the functional groups HO-C=O, C=O and C-OH, respectively.[34, 35] It is worthwhile to note that the samples derived from water steam carbonization display higher O 1s peak intensity than sample derived from the carbonization in argon, indicating that water steam treatment successfully incorporates oxygen species into the resulting composites. The spectra for N species exhibit an intense peak at 398.7 eV and a less intense peak at about 400.6eV (see Fig. 4e), indicating the formation of highly coordinated quaternary 'pyrrolic' N atoms (400.6 eV) incorporated into graphene sheets, along with pyridine-like N atoms incorporated into graphene sheets (398.7 eV).[27] As shown in Fig. 4d, the C 1s spectrum of the samples exhibits a main peak at 284.9 eV, consistent with sp^2 carbon. In addition, the C 1s spectrum can be further deconvoluted into peaks positioned at 284.8, 285.8 and 287.7 eV, which may attributed to C=C, C=N/C-O and C-N/C=O respectively.[29, 34, 35] Based on these XPS analysis and above-mentioned XRD results, we believe that the products derived from the carbonization of ZIF-8 under various conditions are basically N-doped carbon and ZnO composites.

The elemental analysis results of the composites based on EDX analysis are presented in Table 1. The N content for ZnO/C-S samples derived from carbonization under water steam is

in the range of 11.6 to 8.1 wt%, remarkably lower than that for sample ZnO/C-A which was generated via carbonization under argon atmosphere and exhibits the highest N content of 16.5 wt%, possibly due to the high volatility of N species under water steam atmosphere. Actually the N content in sample ZnO/C-S-*S* is only half of that in sample ZnO/C-A. In addition, the bulk N content is very close to its surface content obtained from XPS (i.e., 8.1 and 7.8 wt% for sample ZnO/C-S-*S* obtained via EDX and XPS analysis, respectively), implying the homogenous dispersion of N species in the resulting composites.

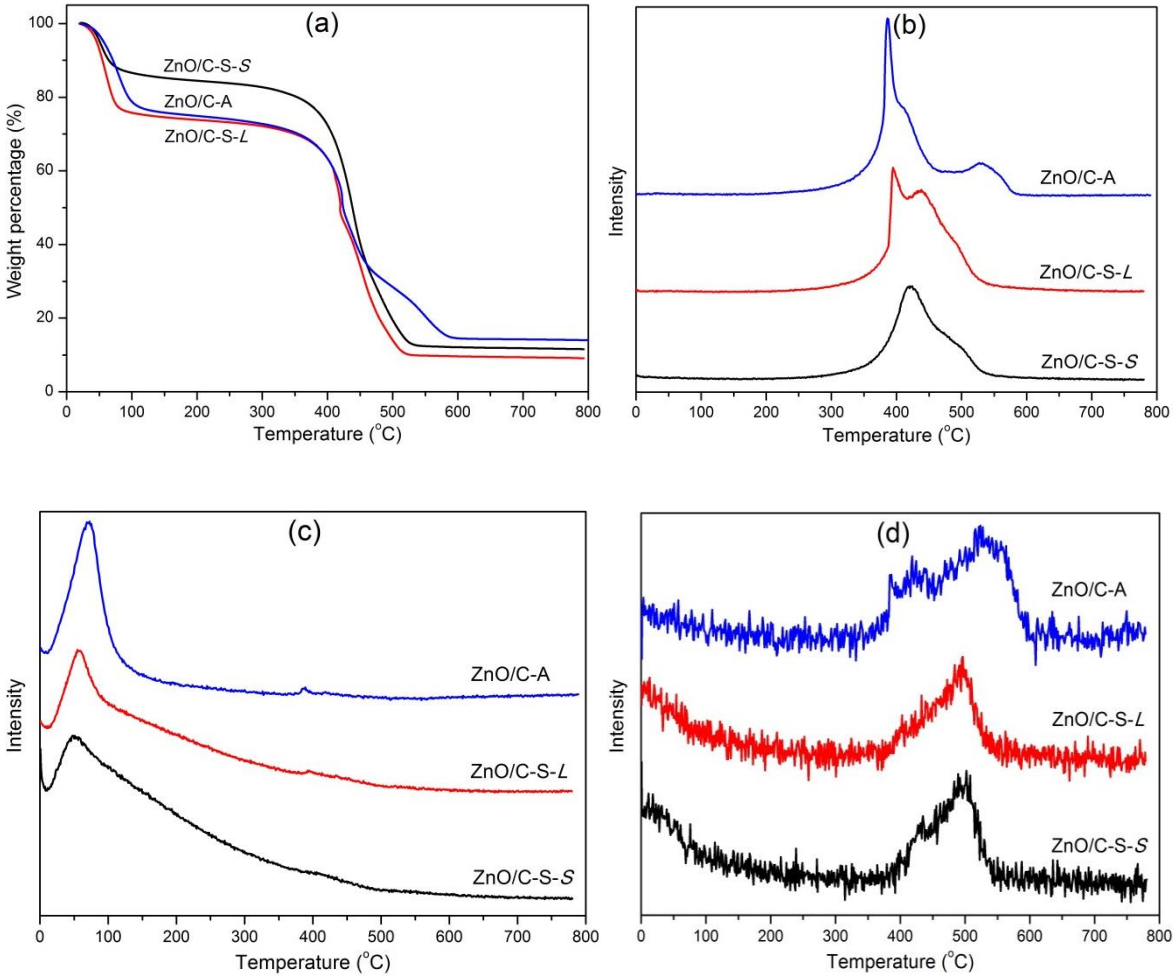

Fig. 5 - TGA (a) and their corresponding MS curves for CO_2 (b), H_2O (c) and NO_2 (d) for different composites.

In addition, the photoluminescence (PL) properties for ZnO/C-S-*S*, ZnO/C-S-*L*, ZnO/C-A and ZnO were evaluated (as shown in Fig. S2) and the ZnO obtained via annealing of ZIF-8 in air shows an intensive PL peak at around 520 nm which is caused by oxygen vacancies. However, the PL intensity of ZnO/C-S-*S*, ZnO/C-S-*L* and ZnO/C-A significantly decreased, suggesting that the excited electrons from ZnO can be transferred to the carbon phase.[18] This phenomenon, quenching in emission of ZnO/C-S-*S*, ZnO/C-S-*L* and ZnO/C-A, also indicates samples ZnO/C-S-*S*, ZnO/C-S-*L* and ZnO/C-A have much better photocatalytic activity than the pure ZnO, as observed in the following photocatalytic measurements.

The thermal stabilities of the composites in air were evaluated by TGA-MS. As shown in Fig. 5a of the TGA profiles, all the composites exhibit a major weight loss event below 100 ^{o}C, corresponding to the removal of adsorbed water from the composites (Fig. 5c). Moreover, composites ZnO/C-S-*S* and ZnO/C-S-*L* derived from the carbonization of ZIF-8 under water steam display a single weight loss event centred at 410–490 ^{o}C, which arises from the burn off the N-doped carbon species in air, as confirmed by the emission of CO_2, NO_2 and trace amount of H_2O in their MS signals (see Fig. 5b and d). However, the composite ZnO/C-A derived from the carbonization of ZIF-8 under argon atmosphere exhibits two weight loss events centred at 400 and 510 ^{o}C, due to the burning off N-doped carbons. Obviously, composites ZnO/C-S-*S* and ZnO/C-S-*L* retain lower residual than composite ZnO/C-A after TGA measurement in air and the residuals are dominated by ZnO.[27] The general lower residual ZnO content (in the range of 10-16%) may be attributed to the fact that ZnO was reduced to metallic Zn by the formed carbon during the carbonization, and the formed Zn would evaporate during the high temperature process since Zn has a relative low boiling point (907 ^{o}C).

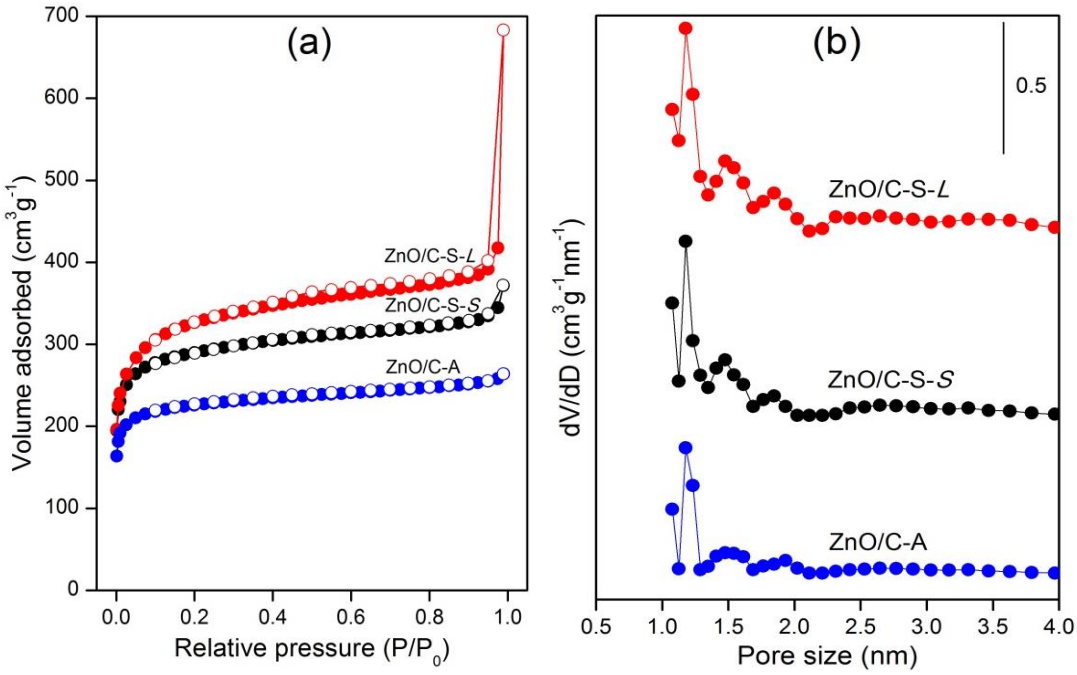

Fig. 6 - N_2 sorption isotherms (a) and the corresponding pore size distribution curves (b) of different porous composite samples.

The textural characteristics of the as-synthesized composites are analysed by N_2 sorption at -196 ^{o}C and the results are summarized in Table 1. As shown in Fig. 6a, the N_2 sorption of the as-synthesized composites all exhibit type I isotherms with significant adsorptions below the relative pressure (P/P_0) = 0.1, due to the capillary filling of micropores. The isotherms for all the composites are similar, and the adsorption–desorption isotherm branches are generally reversible, confirming their predominant microporous feature. Sample ZnO/C-S-*S*, ZnO/C-S-*L* and ZnO/C-A has a specific surface area of 995, 1134 and 771 $m^2 g^{-1}$ and pore volume of 0.58, 1.06 and 0.41 $cm^3 g^{-1}$, respectively, slightly lower than that of the precursor ZIF-8 (Fig. S1c). It is worth noting that, compared with composite derived from carbonization in Ar, the composites derived from water steam carbonization exhibit 29-47% increase in specific surface area and up to 1.5 times improving in pore volume, indicating water steam carbonization can

remarkably improve the surface area and pore volume of the resulting ZnO/C-S composites. Moreover, all the composites display high micropore surface areas (706–986 m^2 g^{-1}) and micropore volumes (0.33–0.45 cm^3 g^{-1}), originating from the high level of zeolite-type pore ordering of ZIF-8 which acts as both the template and the carbon precursor. The proportion of micropore surface areas for all the composites is around 90%, but the proportion of micropore volumes varies from 42–80%. The pore size distribution (PSD) of the composites is further analysed using a Non-Local Density Functional Theory (NLDFT) model based on N_2 adsorption branch data, and the results show that all the as-synthesized composites possess a relative sharp PSD centred at 1.2 nm, without obvious mesopores (as shown in Fig. 6b). In addition, the formation of supermicropores in the range of 1.3–2.0 nm is clearly observed for these composites and the level of the supermicropores increases with the introduction of water steam, and it seems longer steam carbonization can accelerate the formation of supermicropores, implying that steam atmosphere process can affect not only the surface area and pore volume, but also the pore diameters of the composites. This is different from previous report that the hierarchical porous carbon contains micropores, along with the mesopores and macropores are produced by solvent evaporation during the carbonization of MOFs,[36] while our samples mainly contain micropores, without obvious mesopores or macropores. Clearly, the introduction of the oxygen-containing functional groups via water steam process into the ZnO/C-S-*S* and ZnO/C-S-*L* materials can effectively improve the textural properties of the composites.[37]

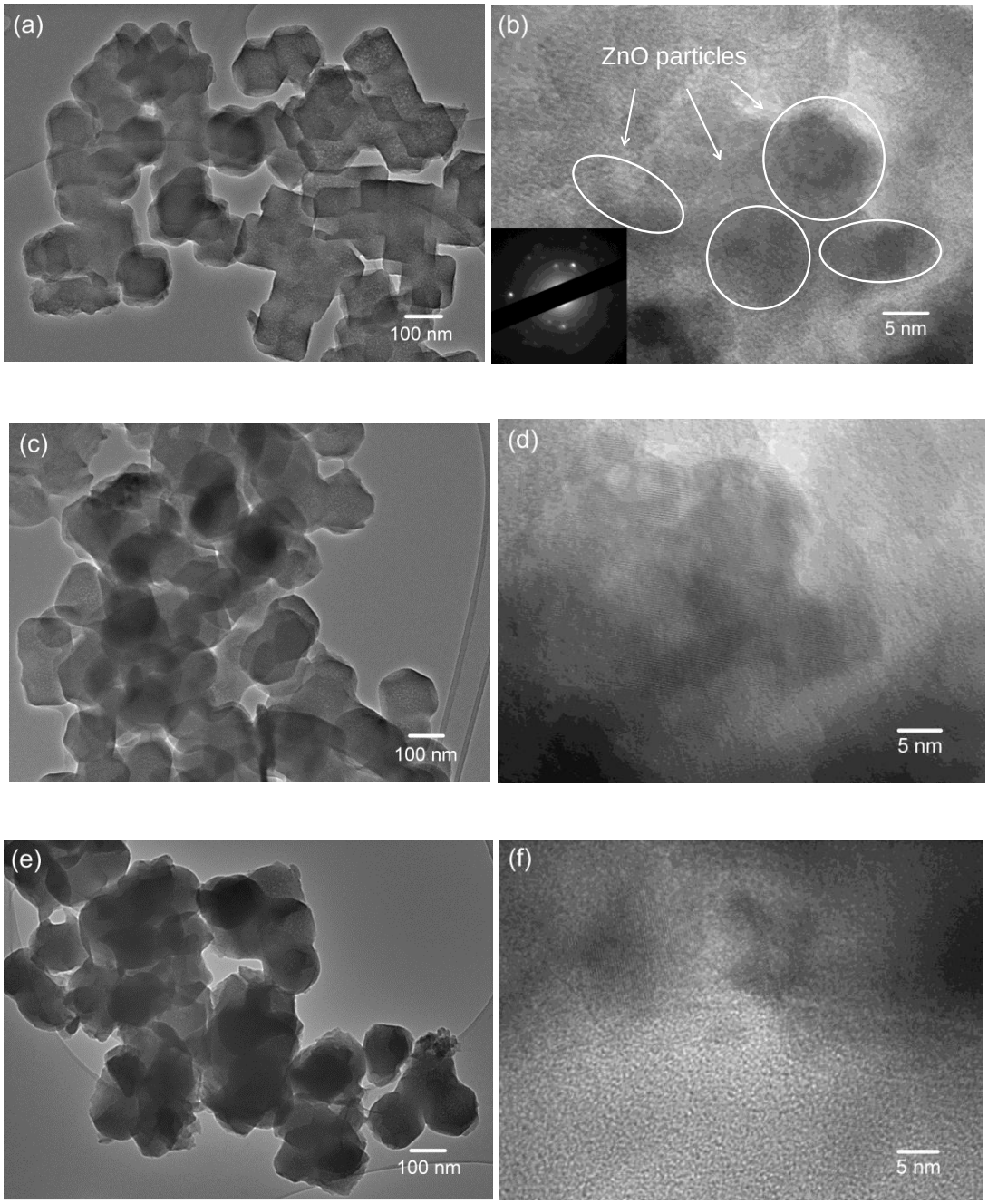

Fig. 7 - Representative TEM images for composite: (a) and (b) ZnO/C-S-*S*, inset showing selected area electronic diffraction patterns, (c) and (d) ZnO/C-S-*L*, and (e) and (f) ZnO/C-A.

TEM analysis is carried out to further investigate the morphologies and microstructures of the resulting porous composites. As shown in Fig. S1b, the ZIF-8 precursor displays the

typical rhombic dodecahedron morphology with an average particle size of 100-150 nm.[27] After carbonization process either in Ar or in steam atmosphere, as presented in Fig. 7, all the ZnO/C composites exhibit spherical-like particles with shrank sizes around 100-130 nm but the small particles tend to agglomeration to form larger particles. It is difficult to observed obvious ZnO particles in low resolution TEM analysis, maybe due to the small particle size of ZnO and confinement effect by carbon. However, under high resolution TEM, the ZnO particles with size in the range of 5-10 nm can be clearly identified (as shown in Fig. 7b and Fig. S3). This is maybe due to the fact that the use of ZIF-8 as a both precursor and template, can result in ZnO nanoparticles formed locally surrounded or coated by porous carbon derived from the carbonization of 2-methylimidazole species in ZIF-8 with arrangement similar to the precursor ZIF-8 structures, leading to homogeneous embedded the ZnO nanoparticles in the porous carbon matrix.[38] In addition, as shown in Fig. 7b, d and f, some pore channels in the carbon domains are distinguishable, with an estimated pore diameter of *ca*. 0.8–1.0 nm, which is consistent with the pore size obtained from N_2 sorption analysis. Selected area electron diffraction (SAED) pattern (inset in Fig. 7b) confirms the formation of crystalline ZnO and amorphous carbon, which is in agreement with the XRD observation in Fig. 1**.**

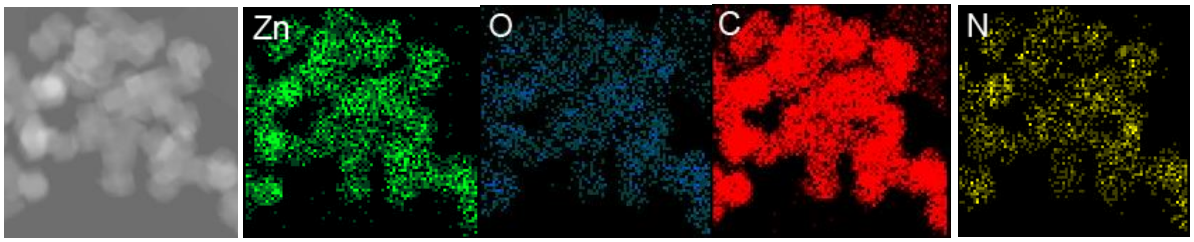

Fig. 8 - Scanning transmission electron microscope image and elemental mapping for sample ZnO/C-S-*S*.

To ascertain the distribution of ZnO nanopartcles in the composite samples, scanning transmission electron microscope combined with elemental mapping technique were used. As shown in Fig. 8, the elemental mapping for both element O and Zn exhibit similar patterns to their selected area of TEM images, indicating the uniform dispersion of ZnO in the carbon matrix. In addition, the elemental mapping for C and N are also similar to their patterns of selected area of TEM image, implying both C and N are uniformly distributed throughout the ZnO/C-S-*S* sample. These results clearly deomonstrated that atomically homogeneous dispersed ZnO/N-doped nanoporous carbon composites is obtained via carbonization of ZIF-8 under water steam carbonization. The reason for the uniform dispersion of ZnO and N-doped carbon is due to the use of a single molecular-like crystalline precursor ZIF-8, whose homogeneously distributed Zn and N ensures their thoroughly distribution on both the external and internal surfaces within the bulk after the carbonization process. In addition, as presented in Fig. S4 and S5, other composites, ZnO/C-S-*L* and ZnO/C-A, also showed homogeneous elemental distrubution throughout the samples, suggesting the formation of atomically and uniformly dispersed ZnO/N-doped carbon composites.

3.2 CO_2 uptake perfomance

To evaluate the appliations of the obtained ZnO/N-doped porous carbon composites, CO_2 adsorption capacities at 25 ^oC for all the samples are presented in Fig. 9a and the CO_2 uptake capacities at 1 bar are summarized in Table 1. The CO_2 adsorption data is confirmed to be highly reproducible, almost identical over several runs, with variations usually lower than 1% in uptake capacity through the entire pressure range. At 25 ^oC and 1 bar, the CO_2 adsorption capacities for samples ZnO/C-A, ZnO/C-S-*S* and ZnO/C-S-*L* are 2.85, 3.05 and 3.23 mmol g^{-1}, which is generally consistent with the gradually increased specific surface areas of these

composites. Therefore, sample ZnO/C-S-*L* derived from steam carbonization for longer time shows the highest CO_2 uptake at 1 bar amongst these composites. However, under low pressures, the ZnO/C-A sample with lower surface area but higher N content out-performs the samples ZnO/C-S-*S* and ZnO/C-S-*L* with higher specific surface area but lower N content in the CO_2 uptake, implying that both specific surface area and N content play important roles in the CO_2 adsorption process at 25 ^{o}C, which is consistent with previous reports.[27, 39] Moreover, as shown in Fig. S6 and Table 1, the CO_2 adsorption capacities at 0 ^{o}C and 1 bar for composites ZnO/C-S-*L*, ZnO/C-S-*S* and ZnO/C-A, are 6.08, 5.32 and 4.42 mmol g^{-1} respectively, which is in agreement well with the observed change trends for CO_2 uptake at 25 ^{o}C. Obviously, the longer steam carbonised sample ZnO/C-S-*L* exhbities the highest CO_2 uptake at 1 bar and 0 ^{o}C amongst the three studied composites. It is, however, worthwhile to note that under low pressures, the CO_2 uptake capacity at 0 ^{o}C for sample ZnO/C-A out-performs that for samples ZnO/C-S-*S*, but lower than that for sample ZnO/C-S-*L*, indicating that textural properties as well as surface chemistry (with different functional groups) can remarkably affect CO_2 adsorption. Actually, surface modification is important for CO_2 adsorption. When water steam was used during the carbonization process, hydrophilic oxygen-containing functional groups such as –OH and –COOH can be introduced onto the surface of ZnO/C-S-*S* and ZnO/C-S-*L* composites, which may benefit to the enhancement of the interaction between the adsorbents with CO_2 molecules.

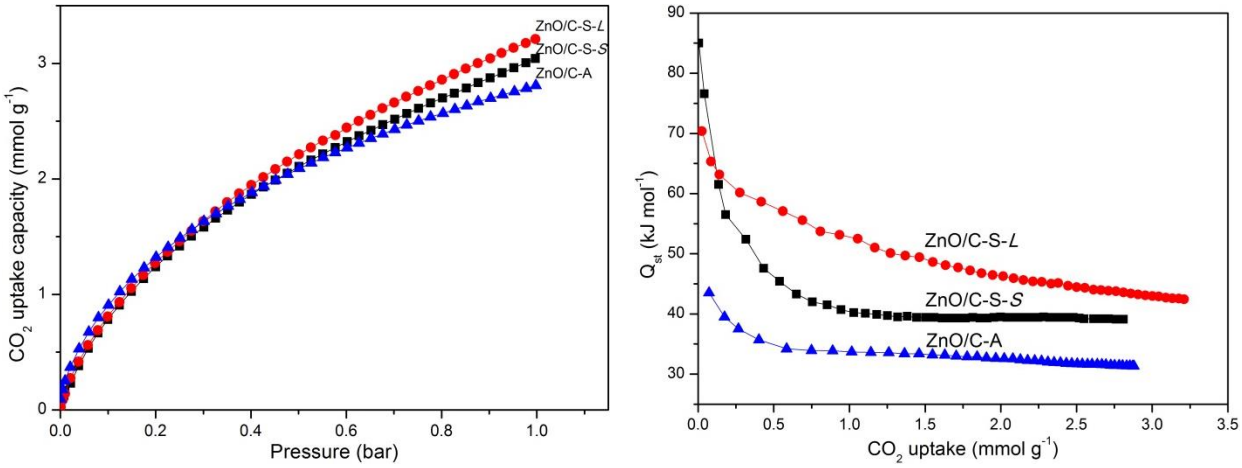

Fig. 9 - CO_2 adsorption capacities at 25 ^oC (a) and the CO_2 isosteric heat Q_{st} (b) for the composite ZnO/C-S-*S*, ZnO/C-S-*L*, and ZnO/C-A.

The CO_2 adsorption energy (i.e., isosteric heat of adsorption, Q_{st}), an indicator of the interaction strength between CO_2 molecules and the adsorbents, is calculated using the CO_2 sorption isotherms measured at 0 and 25 ^oC based on the Clausius–Clapeyron equation for all the samples, and the resulting curves of Q_{st} *vs* CO_2 uptake are presented in Fig. 9b. The initial Q_{st} for the ZnO/C-A, ZnO/C-S-*S* and ZnO/C-S-*L* materials is 44, 85 and 70 kJ mol^{-1}, respectively, at lower CO_2 uptake (low surface coverages). The adsorption Q_{st} of ZnO/C-A is similar to previous observations on other typical N-doped porous carbon materials, but higher than those of most MOFs.[39, 40] This high initial Q_{st} values indicate a strong interaction between CO_2 molecules and the N-doped carbon.[27] Surprisingly, the CO_2 adsorption Q_{st} of ZnO/C-S-*S* and ZnO/C-S-*L* display significant high values, suggesting much stronger interactions between CO_2 molecules and steam carbonised samples than Ar atmosphere carbonised sample ZnO/C-A. This is maybe due to the fact that when CO_2 was adsorbed by samples ZnO/C-S-*S* and ZnO/C-S-*L*, a strong acid-base interaction may have occurred between the hydrophilic oxygen-containing functional groups and the acidic CO_2 molecules.

Furthermore, ZnO may also play an important role in the initial interaction, by forming a strong chemical interaction between ZnO nanoparticles and CO_2 molecules when CO_2 is chemisorbed onto its surfaces.[41-43] Although the mechanism of the chemical interaction between them is yet to fully understand, it is believed the chemisorption of CO_2 on ZnO resulting in the formation of CO_3^{2-} carbonate,[44] which increases the interactions between the adsorbents and CO_2.

At higher coverages, the Q_{st} of the ZnO/C-A, ZnO/C-S-*S* and ZnO/C-S-*L* materials reduces to an average of 32, 39, and 42 kJ mol^{-1}, respectively, which is much higher than previously reported values for pure carbon and N-doped carbon absorbents.[39, 45] Sample ZnO/C-S-*L* that has the longest steam treatment time and intermediate N content, the highest textural properties and CO_2 uptake capacity, exhibits the highest Q_{st} of 42 kJ mol^{-1} at higher coverages, which is actually the highest ever reported for any porous carbon based materials. Sample ZnO/C-S-*S*, possessing shorter steam treatment time, the intermediate specific surface area and intermediate N content, exhibits a Q_{st} of 39 kJ mol^{-1} at high coverages. However, sample ZnO/C-A, which has a higher N content and lower textural properties but without steam treatment, shows the lowest Q_{st} of 32 kJ mol^{-1} at high coverages. These results suggest that at higher CO_2 coverages, both the textural properties and water steam treatment determined the interactions between CO_2 and composites.

To illustrate the adsorption selectivity of the materials, CO_2 uptake against N_2 sorption (shown in Fig. S7) on the materials were performed. At ambient temperature and pressure, CO_2 adsorption capacity on sample ZnO/C-S-*S* (3.05 mmol g^{-1}) is much higher than that of N_2 (0.18 mmol g^{-1}), which results in the CO_2/ N_2 adsorption ratio on sample ZnO/C-S-*S* is 16.9. Similar CO_2/ N_2 adsorption ratio on sample ZnO/C-S-*L* and ZnO/C-A (17.7 and 15.7, respectively) is also observed, implying good selectivity for CO_2 uptake on the synthesized nanocomposites.

The high uptake capacity and good selectivity for CO_2 render these nanocomposites to be promising CO_2 absorbents.

3.3 Removal of methyl blue from water

The porous carbons embedding with ZnO nanoparticles are frequently considered as efficient materials in adsorption and photodegradation of a toxic model substance, methylene blue (MB), under visible-light irradation.[17, 18] To evaluate the capability to removal of MB pollutant from water, the adsorption performance of different samples were first carried out in dark room. As shown in Fig. 10a, the time dependence of the percentage of the adsorbed MB amounts on ZnO/C-S-*S*, ZnO/C-S-*L*, ZnO/C-A and pure ZnO is presented. Except pure ZnO, all the as-synthesized composite samples adsorb MB in dark with the uptake levels depending on the adsorption time, which indicates the carbon matrix plays the key role in the adsorption of MB in dark. After 4 h, composites ZnO/C-A, ZnO/C-S-*S* and ZnO/C-S-*L* can adsorbe 46, 67 and 64% MB from water solution respectively. Moreover, both samples ZnO/C-S-*S* and ZnO/C-S-*L* showed a similar uptake curve with higher adsorption capacities than sample ZnO/C-A. In addition, all the composites ZnO/C-S-*S*, ZnO/C-S-*L* and ZnO/C-A exhibite rapid adsorption perforance in the first 1 h, then the adsorption gradually slowed down till approaching their adsorption/desorption equilibrium. The inset Fig. 10a showed the time-dependent adsorption capacities of ZnO/C-S-*S* and ZnO/C-S-*L*, where ZnO/C-S-*S* and ZnO/C-S-*L* present impressive equilibrium MB dye adsorption capacity of 99 and 97 mg g^{-1}, respectively.

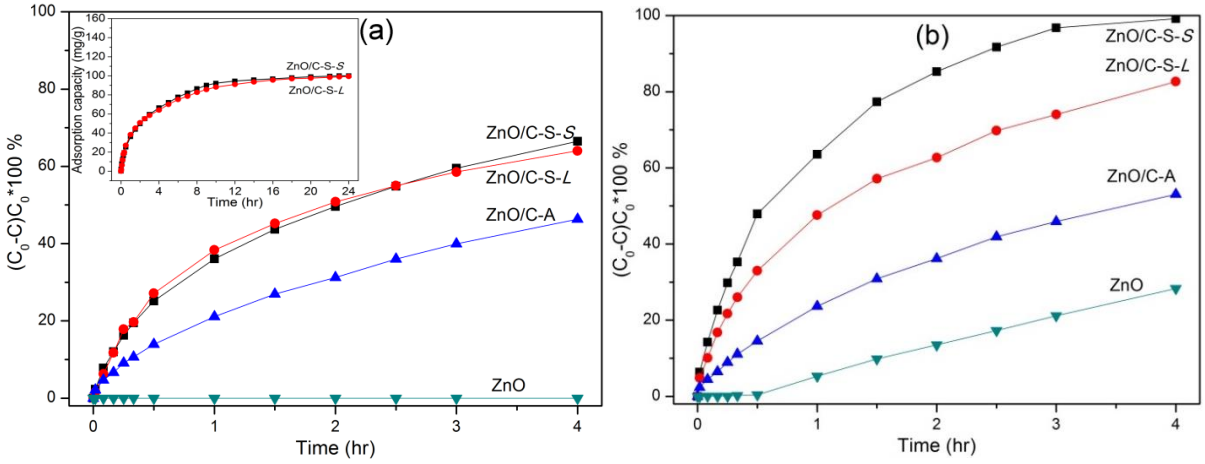

Fig. 10 - The adsorption/photodegradation performances of the samples for the removal of methylene blue from water in dark room (inset: adsorption capacity) (a) and under visible light irradiation (b).

The good adsorption performance of the composites can be accounted for by several factors, including the surface charge, hydrophilicity/hydrophobicity, and textural properties of the composite substrates. The high nanoporosity and open pore network of the carbon matrix can facilitate fast molecular diffusion, improving the accessibility to the entire pore surface. MB has a dimensional size of 1.43 nm × 0.61 nm × 0.4 nm, which is compatible with the pore ranges of 1.2 to 2.0 nm for the ZnO/C composites obtained via the NLDFT method from N_2 gas sorption analysis (Fig. 6). Thus, the matched pore diameters can easily facilitate the diffusion of MB molecules into the carbon matrices. Moreover, the MB dye can interact effectively with the carbon surface, due to the π–π interaction between the MB molecule and the sp^2 graphitic carbon in the ZnO/C composites (as confirmed by Raman analysis in Fig. 3).[46] In addition, the formed -COOH groups on the pore surfaces of the ZnO/C-S-*S* and ZnO/C-S-*L*, which were introduced by water steam carbonization, may also increase the interactions with the MB molecules.[47]

Table 2 - Kinetic parameters of the pseudo-first-order rate equation and the pseudo-second-order rate equation for MB adsorption on as-synthesized porous carbon-zinc oxide composites.

Samples	Pseudo-first-order kinetics			Pseudo-second-order kinetics		
	k_1 /min^{-1}	Q_e / mg g^{-1}	R^2	k_2 / g mg^{-1} min^{-1}	Q_e / mg g^{-1}	R^2
ZnO/C-S-*S*	0.0166	88.69	0.9322	0.00009	105.72	0.9739
ZnO/C-S-*L*	0.0189	82.14	0.9488	0.00011	97.56	0.9891
ZnO/C-A	0.0221	48.95	0.9557	0.00019	59.00	0.9873

Further adsorption kinetics analyses are carried out, using the pseudo-first-order and pseudo-second-order kinetic model,[48] in an effort to understand the adsorption mechanism. The pseudo-first-order equation is given as follows:

$$\log(Q_e - Q_t) = logQ_e - \frac{k_1}{2.303}t$$

where k_1 (min^{-1}) is the adsorption rate constant of pseudo-first-order model, Q_e (mg g^{-1}) and Q_t (mg g^{-1}) are the amount on adsorbent at equilibrium and time t, respectively.

The pseudo-second-order rate reaction is dependent on the amount of solute adsorbed on the surface of the adsorbent and the amount adsorbed at equilibrium.The pseudo-second-order equation is given as follows:

$$\frac{t}{Q_t} = \frac{1}{k_2 Q_e^2} + \frac{t}{Q_e}$$

where k_2 (g mg^{-1} min^{-1}) is the adsorption rate constant for the pseudo-second-order adsorption; Q_e (mg g^{-1}) and Q_t (mg g^{-1}) are the amount of solute adsorbed at equilibrium and at time t.

The linear plots of $\log(Q_e - Q_t)$ *vs. t* and (t/Q_t) *vs. t* are drawn for the pseudo-first-order and pseudo-second-order models, respectively (See Fig. S8). The adsorption rate constants k_1 and k_2 can be obtained from the plot of experimental data. The adsorption rate constants, the calculated Q_e, and the correlation coefficients R^2 for the two kinetic models of the as-synthesized materials are summarized in Table 2. As seen from Table 2, the correlation coefficients (R^2) of the pseudo-first-order model are 0.932, 0.949 and 0.956 for ZnO/C-S-*S*, ZnO/C-S-*L* and ZnO/C-A, respectively. For the pseudo-second-order model, the correlation coefficients (R^2) of the ZnO/C-S-*S*, ZnO/C-S-*L* and ZnO/C-A are all higher than 0.97. In addition, in the case of the pseudo-first-order model, the calcualted Q_e values were 88.69 mg g^{-1} for ZnO/C-S-*S* and 82.14 mg g^{-1} ZnO/C-S-*L*. On the other hand, the calculated Q_e values from the pseudo-second-order model for the adsorption of MB by ZnO/C-S-*S* and ZnO/C-S-*L* were 105.72 and 97.56 mg g^{-1}, respectively. Obviously, the calculated Q_e values from the pseudo-second-order model are in well agreement with the experimental measured data (shown in Fig. 10a). It is therefore reasonable to assume that the adsorption of MB on these composites is dominated by the pseudo-second-order model, rather than the pseudo-first-order model. This observation is consistent with the above discussed the adsorption of MB on the composites is mainly a process of MB interaction with the various functional sites of the composites.

ZnO, a direct wide band gap (3.37 eV) semiconductor with a large excitation binding energy (60 meV), has been investigated as a potential non-toxic photocatalyst to degrade organic pollutants.[49, 50] The adsorption and degradation of MB from water for different samples under visible light irradiation are presented in Fig. 10b. After 4 h irradiation, up to 99, 83, 53 and 28 % MB has been removed from water by samples ZnO/C-S-*S*, ZnO/C-S-*L*,

ZnO/C-A and pure ZnO respectively, which indicates that photo-degradation contributes to 32, 19, 7 and 28% of the MB removal, respectively. Considering that only 10, 13 and 15% ZnO exisit in the obtained composite ZnO/C-S-*L*, ZnO/C-S-*S* and ZnO/C-A respectively, the photo-degradation efficiency of ZnO in all composites outperform the pure ZnO in their photocatalytic removal of MB from water. This is due to the fact that carbon species in the composites can effectively modify the bandgaps of ZnO, generate localized states in the bandgap which results in the presence of an absorption tail extending into the visible range.[51] It is worth noting that a commercial ZnO (size ~200 nm) exhibited the similar photocatalytic activity (shown in Fig. S9) with the pure ZnO obtained from annealing of ZIF-8 in air, while another commercial material TiO_2 (P25) showed no photocatalytic activity under visible light radiation, which is consistent with the fact that P25 is photocatalytic activity under UV radiation instead of visible light.[52]

Consequently, the carbon species in ZnO/C composite promotes the photodegradation performance. Moreover, compared to the sample ZnO/C-A obtained from the carbonization of ZIF-8 in Ar atmosphere, the composites ZnO/C-S-*L* and ZnO/C-S-*S* derived from steam carbonization possessing abundant hydrophilic oxygen-containing functional groups may facilitate the approaching and accommodating of MB molecules, which may result in samples ZnO/C-S-*L* and ZnO/C-S-*S* exhibit higher photo-degradation performances than ZnO/C-A. In addition, composite ZnO/C-S-*S* out-performs the composite ZnO/C-S-*L* in photo-degradation of MB in water due to the higher ZnO content in the former sample.

The reusability of sample ZnO/C-S-*S* is also assessed for the removal of MB from water under visible-light irradiation. In the consecutive tests, the composite catalysts were separated from the solution by filtration, washed several times with deionized water, followed by dried in oven at 120 ^{o}C for 3 h and then used for the next run. As shown in Fig. 11, the MB removal efficiency was remain high and still higher than 95% after six consecutive runs, suggesting a

good stability and reusability for the ZnO/C-S-*S* materials. It is likely that the physical walls of the porous carbon provide a confined space for photocatalysis,[15] which can prevent the aggregation of ZnO nanoparticles, maintain the high dispersibility of ZnO particles in porous carbon matrix, therefore the composite materials can keep the high adsorption and degradation activity and enhance the stability for MB removal from water.

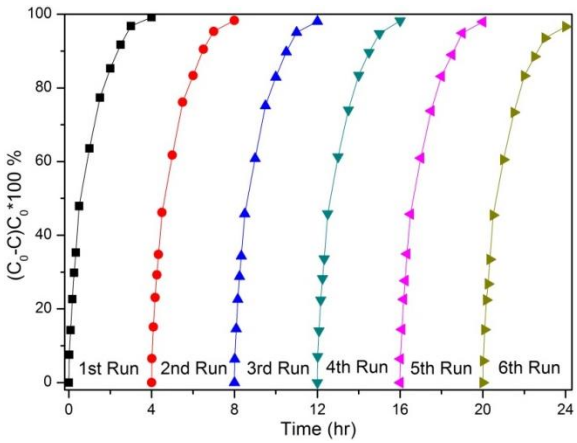

Fig. 11 - Reuse of the composite ZnO/C-S-*S* in the adsorption and photodegradation of MB in water under visible-light irradiation.

4. Conclusions

In summary, we have successfully developed a simple one-step water steam carbonization route to synthesize ZnO nanocrystal particles homogeneously embedded within N-doped porous carbon matrix using ZIF-8 as a precursor. This new and green method holds several advantages: (1) the porosity of composites can be significantly improved; (2) the crystallinity of metal oxide is remarkably increased and (3) abundant oxygen-containing hydrophilic

functional groups have been introduced into the N-doped porous carbon in the composites. The resultants ZnO/C-S-*S* and ZnO/C-S-*L* exhibit promising CO_2 uptake capacities, high CO_2 selectivity, with a remarkable high CO_2 adsorption energy at low surface coverages due to the high porosity, high N content and a strong chemical interaction between CO_2 and the composites. Furthermore, with excellent adsorption and degradation abilities, these composites are also highly efficient for methylene blue (MB) removal from wastewater under visible-light irradiation, which can be attributed to the high porosity, additional functional groups, open network structure of the carbon matrix and the excellent photocatalytic performance of ZnO nanocrystals. Kinetics studies show that the adsorption process is dominated with a pseudo-second-order adsorption model. This present work offers a new approach for the design and syntheses of highly homogeneous dispersed metal oxide/porous carbon composite materials that display enhanced sorption and efficient catalytic behaviours.

Acknowledgements

The authors are grateful to the Royal Society, the Royal Academy of Engineering and University of Exeter for financial supports.

Appendix A. Supplementary data

Supplementary data associated with this article can be found in the online version.

REFERENCES

[1] Gu D, Bongard H, Deng Y, Feng D, Wu Z, Fang Y, et al. An aqueous emulsion route to synthesize mesoporous carbon vesicles and their nanocomposites. Adv Mater 2010;22(7):833-7.

[2] Wu Z, Zhao D. Ordered mesoporous materials as adsorbents. Chem Commun 2011;47(12):3332-8.

[3] Liu J, Qiao SZ, Liu H, Chen J, Orpe A, Zhao D, et al. Extension of the Stober method to the preparation of monodisperse resorcinol-formaldehyde resin polymer and carbon spheres. Angew Chem Int Ed 2011;50(26):5947-51.

[4] Yang T, Liu J, Zheng Y, Monteiro MJ, Qiao SZ. Facile fabrication of core-shell-structured Ag@carbon and mesoporous yolk-shell-structured Ag@carbon@silica by an extended Stober method. Chem Eur J 2013;19(22):6942-5.

[5] Xia YD, Yang ZX, Zhu YQ. Porous carbon-based materials for hydrogen storage: advancement and challenges. J Mater Chem A 2013;1(33):9365-81.

[6] Joo SH, Choi SJ, Oh I, Kwak J, Liu Z, Terasaki O, et al. Ordered nanoporous arrays of carbon supporting high dispersions of platinum nanoparticles. Nature 2001;412(6843):169-72.

[7] Liu L, Deng QF, Agula B, Zhao X, Ren TZ, Yuan ZY. Ordered mesoporous carbon catalyst for dehydrogenation of propane to propylene. Chem Commun 2011;47(29):8334-6.

[8] Yang ZX, Xia YD, Mokaya R. Zeolite ZSM-5 with unique supermicropores synthesized using mesoporous carbon as a template. Adv Mater 2004;16(8):727-32.

[9] Biener J, Stadermann M, Suss M, Worsley MA, Biener MM, Rose KA, et al. Advanced carbon aerogels for energy applications. Energy Environ Sci 2011;4(3):656-67.

[10] Gogotsi Y, Nikitin A, Ye H, Zhou W, Fischer JE, Yi B, et al. Nanoporous carbide-derived carbon with tunable pore size. Nat Mater 2003;2(9):591-4.

[11] Xia Y, Yang Z, Mokaya R. Templated nanoscale porous carbons. Nanoscale 2010;2(5):639-59.

[12] Liu WJ, Jiang H, Tian K, Ding YW, Yu HQ. Mesoporous carbon stabilized MgO nanoparticles synthesized by pyrolysis of $MgCl_2$ preloaded waste biomass for highly efficient CO_2 capture. Environ Sci Technol 2013;47(16):9397-403.

[13] Bhagiyalakshmi M, Hemalatha P, Ganesh M, Mei PM, Jang HT. A direct synthesis of mesoporous carbon supported MgO sorbent for CO_2 capture. Fuel 2011;90(4):1662-7.

[14] Kochuveedu ST, Jang YJ, Jang YH, Lee WJ, Cha MA, Shin H, et al. Visible-light active nanohybrid TiO_2/carbon photocatalysts with programmed morphology by direct carbonization of block copolymer templates. Green Chem 2011;13(12):3397-405.

[15] Wei W, Yu C, Zhao Q, Li G, Wan Y. Improvement of the visible-light photocatalytic performance of TiO_2 by carbon mesostructures. Chem Eur J 2013;19(2):566-77.

[16] Xue G, Liu H, Chen Q, Hills C, Tyrer M, Innocent F. Synergy between surface adsorption and photocatalysis during degradation of humic acid on TiO_2/activated carbon composites. J Hazard Mater 2011;186(1):765-72.

[17] Wang F, Liang L, Shi L, Liu M, Sun J. CO_2-assisted synthesis of mesoporous carbon/C-doped ZnO composites for enhanced photocatalytic performance under visible light. Dalton Trans 2014;43(43):16441-9.

[18] Kochuveedu ST, Jang YH, Jang YJ, Kim DH. Visible light active photocatalysis on block copolymer induced strings of ZnO nanoparticles doped with carbon. J Mater Chem A 2013;1(3):898-905.

[19] Chen BL, Yang ZX, Zhu YQ, Xia YD. Zeolitic imidazolate framework materials: recent progress in synthesis and applications. J Mater Chem A 2014;2(40):16811-31.

[20] Phan A, Doonan CJ, Uribe-Romo FJ, Knobler CB, O'Keeffe M, Yaghi OM. Synthesis, structure, and carbon dioxide capture properties of zeolitic imidazolate frameworks. Acc Chem Res 2010;43(1):58-67.

[21] Sun JK, Xu Q. Functional materials derived from open framework templates/precursors: synthesis and applications. Energy Environ Sci 2014;7(7):2071-100.

[22] Chaikittisilp W, Ariga K, Yamauchi Y. A new family of carbon materials: synthesis of MOF-derived nanoporous carbons and their promising applications. J Mater Chem A 2013;1(1):14-9.

[23] Das R, Pachfule P, Banerjee R, Poddar P. Metal and metal oxide nanoparticle synthesis from metal organic frameworks (MOFs): finding the border of metal and metal oxides. Nanoscale 2012;4(2):591-9.

[24] Chaikittisilp W, Torad NL, Li C, Imura M, Suzuki N, Ishihara S, et al. Synthesis of nanoporous carbon-cobalt-oxide hybrid electrocatalysts by thermal conversion of metal-organic frameworks. Chem Eur J 2014;20(15):4217-21.

[25] Zhang GJ, Li CX, Liu J, Zhou L, Liu RH, Han X, et al. One-step conversion from metal-organic frameworks to Co_3O_4@N-doped carbon nanocomposites towards highly efficient oxygen reduction catalysts. J Mater Chem A 2014;2(22):8184-9.

[26] Park KS, Ni Z, Cote AP, Choi JY, Huang R, Uribe-Romo FJ, et al. Exceptional chemical and thermal stability of zeolitic imidazolate frameworks. Proc Natl Acad Sci USA 2006;103(27):10186-91.

[27] Bai FH, Xia YD, Chen BL, Su HQ, Zhu YQ. Preparation and carbon dioxide uptake capacity of N-doped porous carbon materials derived from direct carbonization of zeolitic imidazolate framework. Carbon 2014;79:213-26.

[28] Cravillon J, Munzer S, Lohmeier SJ, Feldhoff A, Huber K, Wiebcke M. Rapid room-temperature synthesis and characterization of nanocrystals of a prototypical zeolitic imidazolate framework. Chem Mater 2009;21(8):1410-2.

[29] Zhong HX, Wang J, Zhang YW, Xu WL, Xing W, Xu D, et al. ZIF-8 derived graphene-based nitrogen-doped porous carbon sheets as highly efficient and durable oxygen reduction electrocatalysts. Angew Chem Int Ed 2014;53(51):14235-9.

[30] Ferrari AC. Raman spectroscopy of graphene and graphite: Disorder, electron–phonon coupling, doping and nonadiabatic effects. Solid State Commun 2007;143(1-2):47-57.

[31] Castiglioni C, Negri F, Rigolio M, Zerbi G. Raman activation in disordered graphites of the A_1' symmetry forbidden $k\neq0$ phonon: The origin of the D line. The J Chem Phys 2001;115(8):3769.

[32] Li Z, Xu ZW, Tan XH, Wang HL, Holt CMB, Stephenson T, et al. Mesoporous nitrogen-rich carbons derived from protein for ultra-high capacity battery anodes and supercapacitors. Energy Environ Sci 2013;6(3):871-8.

[33] Kotsis K, Staemmler V. Ab initio calculations of the O1s XPS spectra of ZnO and Zn oxo compounds. Phys Chem Chem Phys 2006;8(13):1490-8.

[34] Yang SB, Zhi LJ, Tang K, Feng XL, Maier J, Mullen K. Efficient synthesis of heteroatom (N or S)-doped graphene based on ultrathin graphene oxide-porous silica sheets for oxygen reduction reactions. Adv Funct Mater 2012;22(17):3634-40.

[35] Wang J, Zhong HX, Qin YL, Zhang XB. An efficient three-dimensional oxygen evolution electrode. Angew Chem Int Ed 2013;52(20):5248-53.

[36] Yang SJ, Kim T, Lee K, Kim YS, Yoon J, Park CR. Solvent evaporation mediated preparation of hierarchically porous metal organic framework-derived carbon with controllable and accessible large-scale porosity. Carbon 2014;71(0):294-302.

[37] Xiao ZB, Yang Z, Nie HG, Lu YQ, Yang KQ, Huang SM. Porous carbon nanotubes etched by water steam for high-rate large-capacity lithium-sulfur batteries. J Mater Chem A 2014;2(23):8683-9.

[38] Yang SJ, Nam S, Kim T, Im JH, Jung H, Kang JH, et al. Preparation and exceptional lithium anodic performance of porous carbon-coated ZnO quantum dots derived from a metal-organic framework. J Am Chem Soc 2013;135(20):7394-7.

[39] Xia YD, Mokaya R, Walker GS, Zhu YQ. Superior CO_2 adsorption capacity on N-doped, high-surface-area, microporous carbons templated from zeolite. Adv Energy Mater 2011;1(4):678-83.

[40] Furukawa H, Yaghi OM. Storage of hydrogen, methane, and carbon dioxide in highly porous covalent organic frameworks for clean energy applications. J Am Chem Soc 2009;131(25):8875-83.

[41] Dutta G, Sokol AA, Catlow CR, Keal TW, Sherwood P. Activation of carbon dioxide over zinc oxide by localised electrons. ChemPhysChem 2012;13(15):3453-6.

[42] Yasumoto I. Adsorption of water, ammonia, and carbon-dioxide on ninc-oxide at elevated-temperatures. J Phys Chem 1984;88(18):4041-4.

[43] Kokes RJ, Glemza R. Thermodynamics of adsorption of carbon dioxide on zinc oxide. J Phys Chem 1965;69(1):17-21.

[44] Freund HJ, Roberts MW. Surface chemistry of carbon dioxide. Surf Sci Rep 1996;25(8):225-73.

[45] Sevilla M, Valle-Vigon P, Fuertes AB. N-Doped polypyrrole-based porous carbons for CO_2 capture. Adv Funct Mater 2011;21(14):2781-7.

[46] Torad NL, Hu M, Ishihara S, Sukegawa H, Belik AA, Imura M, et al. Direct synthesis of MOF-derived nanoporous carbon with magnetic Co nanoparticles toward efficient water treatment. Small 2014;10(10):2096-107.

[47] Zhang Q, Yu J, Cai J, Song R, Cui Y, Yang Y, et al. A porous metal-organic framework with -COOH groups for highly efficient pollutant removal. Chem Commun 2014;50(92):14455-8.

[48] Ho YS, McKay G. Pseudo-second order model for sorption processes. Process Biochem 1999;34(5):451-65.

[49] Zhu YP, Li M, Liu YL, Ren TZ, Yuan ZY. Carbon-doped ZnO hybridized homogeneously with graphitic carbon nitride nanocomposites for photocatalysis. J Phys Chem C 2014;118(20):10963-71.

[50] Zou RJ, He GJ, Xu KB, Liu Q, Zhang ZY, Hu JQ. ZnO nanorods on reduced graphene sheets with excellent field emission, gas sensor and photocatalytic properties. J Mater Chem A 2013;1(29):8445-52.

[51] Liu G, Wang LZ, Yang HG, Cheng HM, Lu GQ. Titania-based photocatalysts-crystal growth, doping and heterostructuring. J Mater Chem 2010;20(5):831-43.

[52] Yang SJ, Im JH, Kim T, Lee K, Park CR. MOF-derived ZnO and ZnO@C composites with high photocatalytic activity and adsorption capacity. J Hazard Mater 2011;186(1):376-82.